

Diverse Relationship between ENSO and the Northwest Pacific Summer Climate among CMIP5 Models: Dependence on the ENSO Decay Pace

WENPING JIANG,^{a,e} GANG HUANG,^{a,b,c} KAIMING HU,^{a,b,d} RENGUANG WU,^{a,d} HAINAN GONG,^d
XIAOLONG CHEN,^a AND WEICHEN TAO^{a,e}

^a State Key Laboratory of Numerical Modeling for Atmospheric Sciences and Geophysical Fluid Dynamics,
Institute of Atmospheric Physics, Chinese Academy of Sciences, Beijing, China

^b Joint Center for Global Change Studies, Beijing, China

^c Shenzhen Key Laboratory of Severe Weather in South China, Shenzhen, China

^d Center for Monsoon System Research, Institute of Atmospheric Physics, Chinese Academy
of Sciences, Beijing, China

^e University of Chinese Academy of Sciences, Beijing, China

(Manuscript received 11 May 2016, in final form 6 September 2016)

ABSTRACT

The impacts of El Niño–Southern Oscillation (ENSO) on the northwest Pacific (NWP) climate during ENSO decay summers are investigated based on the outputs of 37 coupled general circulation models (CGCMs) from phase 5 of the Coupled Model Intercomparison Project (CMIP5). Large intermodel spread exists in the 37 state-of-the-art CGCMs in simulating the ENSO–NWP relationship. Eight high-skill and eight low-skill models are selected to explore how the bias arises. By comparing the results among high-skill models, low-skill models, and observations, the simulation skill of the ENSO–NWP relationship largely depends on whether the model can reasonably reproduce the ENSO decay pace. Warm SST anomaly bias in the equatorial western Pacific (EWP) is found to persist into the ENSO decay summer in the low-skill models, obstructing the formation of an anomalous anticyclone in the NWP. Further analysis shows that the warm EWP SST anomaly bias is possibly related to the excessive westward extension of cold tongue in these models, which increases climatological zonal SST gradient in the EWP. Under westerly wind anomalies, the larger climatological zonal SST gradient could lead to warmer zonal advections in the low-skill models than that in the high-skill models, which could lead to warm EWP SST anomaly bias in the low-skill models. And the warm EWP SST anomaly bias could strengthen westerly wind anomalies over the western Pacific by triggering convection and atmospheric Rossby waves, which, in turn, could maintain the warm SST anomaly bias in the EWP.

1. Introduction

The northwest Pacific summer monsoon (NWPSM) is one of the important subcomponents of the global monsoon, and it has considerable impacts on the livelihood of more than one billion people in East Asia. The interannual variability of NWPSM is intrinsically strongly affected by El Niño–Southern Oscillation (ENSO) (Huang and Wu 1989; Chang et al. 2000; Chou

et al. 2009; Lin and Lu 2009; Chen and Zhou 2014). An anomalous northwest Pacific anticyclone (NWPAC), forming in the El Niño mature phase and maintaining in the following spring and summer, is a key system linking ENSO and East Asia climate (Zhang et al. 1999; Lau and Nath 2000; Wang et al. 2000; Zhang and Sumi 2002; Chou et al. 2003; Wang et al. 2003; Wu et al. 2003; Hu et al. 2014). In post-El Niño summers, there are cold and wet anomalies in eastern China and Japan, while precipitation tends to decrease in the subtropical northwest Pacific (NWP) (Zhang et al. 1999; Wang et al. 2000).

Extensive studies have been conducted to investigate the mechanism for the formation and maintenance of anomalous NWPAC. In El Niño mature phase, the change of Walker circulation leads to an anomalous

Corresponding author address: Gang Huang, State Key Laboratory of Numerical Modeling for Atmospheric Sciences and Geophysical Fluid Dynamics, Institute of Atmospheric Physics, Chinese Academy of Sciences, 40 Hua Yan Li, Beijing 100029, China.
E-mail: hg@mail.iap.ac.cn

anticyclone developing in the tropical NWP, and the anticyclone could maintain into the following summer through local wind–evaporation feedback (Wang et al. 2003). Moreover, the El Niño–induced tropical Indian Ocean (TIO) warming could reinforce the anomalous NWPAC through the Indian Ocean capacitor effect (Xie et al. 2009). The TIO warming forces a Matsuno–Gill (Matsuno 1966; Gill 1980) pattern in tropospheric temperature with a Kelvin wave propagating into the tropical western Pacific and induces anomalous NWPAC through Ekman divergence and suppressed convection (Yang et al. 2007; Xie et al. 2009; Yang et al. 2010). The two mechanisms may work together to maintain the NWPAC (Xie et al. 2016). In addition, the tropical Indo–western Pacific sea surface temperature (SST) gradient can also influence the formation of NWPAC anomalies (Terao and Kubota 2005; Chen et al. 2012; Cao et al. 2013; Wu et al. 2014; He and Zhou 2015), which is associated with the duration of El Niño decay phase.

The above results are mainly based on observations. The outputs from phase 5 of the Coupled Model Intercomparison Project (CMIP5) (Taylor et al. 2012) provide a good opportunity to explore the relationship between ENSO and East Asia summer climate using state-of-the-art coupled general circulation models (CGCMs). Previous studies mainly focused on the impacts of the Indian Ocean capacitor effect on the simulation skill of summer climate in East Asia (Hu et al. 2014; Song and Zhou 2014; Tao et al. 2016) and ignored the important impacts of SST anomalies in other regions. Tao et al. (2016) focused on evaluating the effects of the Indian Ocean basin mode in CMIP3/CMIP5. Although Tao et al. (2016) pointed out that the NWPAC bias in the models may be associated with the SST anomalies in the equatorial western Pacific (EWP), they did not provide further analysis and did not explore the source of the SST anomaly bias in the EWP. He and Zhou (2015) indicated that the NWPAC intensity is dominated by the zonal SST gradient between the TIO and the EWP. However, they did not explore the relative impacts of SST anomalies in the two regions on the NWPAC bias in CMIP5 CGCMs. In this paper, we perform more detailed diagnosis and attribution analysis about the NWPAC bias during the ENSO decay summer and find that the NWPAC is more sensitive to SST anomalies in the EWP than to SST anomalies in the TIO and SST anomalies in the local NWP in CMIP5 CGCMs. Furthermore, the causes of SST anomaly bias in the EWP are investigated. This will be helpful to advance the understanding of the model performance and improve the East Asia–NWP summer climate prediction.

The rest of this study is organized as follows. Section 2 provides a brief description of datasets and methods. In section 3, we evaluate the model performance in simulating the relationship between ENSO and NWPSM. Section 4 identifies the primary source of bias in simulation of anomalous NWPAC related to ENSO in CMIP5 CGCMs. Then, we investigate the causes of the major bias in section 5. A summary is presented in section 6.

2. Model, observational datasets, and methods

a. Datasets

The SST used in this study is from the monthly mean historical Extended Reconstructed Sea Surface Temperature, version 3 (ERSST3), dataset (Smith et al. 2008), which has a horizontal resolution of $2^\circ \times 2^\circ$. The oceanic potential temperature and current velocity data are from the Simple Ocean Data Assimilation version 2.2.4 (SODA_2.2.4) (Carton and Giese 2008), and the monthly mean output is mapped onto a uniform $0.5^\circ \times 0.5^\circ \times 40$ -level grid. The monthly mean rainfall is from version 2 of the Global Precipitation Climatology Project (Adler et al. 2003), which is available on a $2.5^\circ \times 2.5^\circ$ grid. The shortwave (SW) and longwave (LW) radiation, latent heat flux (LHF), sensible heat flux (SHF) at sea surface, and zonal wind stress have a resolution of $1.875^\circ \times 1.875^\circ$, which is from the National Centers for Environment Prediction–National Center for Atmospheric Research (NCEP–NCAR) reanalysis (Kalnay et al. 1996). The atmospheric circulation data and air temperature with a resolution of $2.5^\circ \times 2.5^\circ$ are also from the NCEP–NCAR reanalysis.

This study uses monthly mean outputs from historical simulation of 37 CMIP5 coupled models. Brief descriptions of the 37 CMIP5 coupled models including their modeling centers, horizontal resolutions, and vertical levels are listed in Table 1. Monthly mean variables used include SST, precipitation, wind, air temperature, zonal wind stress, downward and upward SW and LW radiation, LHF and SHF at sea surface, oceanic potential temperature, and current velocity. Because of the large number of experiments included in the CMIP5 framework, only one member (r1i1p1) run of each model is analyzed. To help understand the effect of SST anomalies in different regions on the bias, we perform a suite of sensitivity experiments by using CAM4, which is an atmospheric general circulation model (AGCM) from the National Center for Atmospheric Research. Five sets of experiments are implemented including one standard climatological SST run (CAM4_Clim) as a control run and four sensitivity AMIP-type runs. The

TABLE 1. The climate modeling centers, horizontal resolution and vertical levels of 37 CMIP5 models are listed. The high-skill models are denoted by an asterisk, and the low-skill models are denoted by two asterisks.

Model	Institute	Atmospheric resolution
ACCESS1.0	Commonwealth Scientific and Industrial Research Organization (CSIRO) and Bureau of Meteorology (BoM), Australia	192 × 144L38
BCC_CSM1.1	Beijing Climate Center, China Meteorological Administration, China	128 × 64L26
BCC_CSM1.1(m)		320 × 160L26
BNU-ESM*	College of Global Change and Earth System Science, Beijing Normal University, China	128 × 64L26
CanCM4**	Canadian Centre for Climate Modeling and Analysis, Canada	128 × 64L35
CanESM2**		
CCSM4	National Center for Atmospheric Research, United States	288 × 192L26
CESM1(BGC)	Community Earth System Model Contributors, United States	288 × 192L26
CESM1(CAM5)*		288 × 192L30
CESM1(FASTCHEM)		288 × 192L26
CESM1(WACCM)		144 × 96L66
CMCC-CM	Centro Euro-Mediterraneo per I Cambiamenti Climatici, Italy	480 × 240L31
CMCC-CMS		192 × 96L95
CNRM-CM5	Centre National de Recherches Météorologiques and Centre Européenne Recherche et Formation Avancées en Calcul Scientifique, France	256 × 128L31
CSIRO Mk3.6.0**	Queensland Climate Change Centre of Excellence and Commonwealth Scientific and Industrial Research Organization, Australia	192 × 96L18
FGOALS-g2*	LASG, Institute of Atmospheric Physics, Chinese Academy of Sciences and CESS, Tsinghua University, China	128 × 60L26
FGOALS-s2*	LASG, Institute of Atmospheric Physics, China	128 × 108L26
FIO-ESM*	The First Institute of Oceanography, SOA, China	128 × 64L26
GFDL CM2.1*	NOAA Geophysical Fluid Dynamics Laboratory, United States	144 × 90L24
GFDL CM3.0		144 × 90L48
GFDL-ESM2G		144 × 90L24
GFDL-ESM2M*		144 × 90L24
GISS-E2-H	NASA Goddard Institute for Space Studies, United States	144 × 90L40
GISS-E2-R		
HadCM3**	Met Office Hadley Centre, United Kingdom	96 × 73L19
INM-CM4.0**	Institute for Numerical Mathematics, Russia	180 × 120L21
IPSL-CM5A-LR**	Institute Pierre-Simon Laplace, France	96 × 95L39
IPSL-CM5A-MR		144 × 143L39
IPSL-CM5B-LR		96 × 95L39
MIROC5	University of Tokyo, National Institute for Environmental Studies, and Japan Agency for Marine-Earth Science and Technology, Japan	256 × 128L40
MIROC-ESM		128 × 64L80
MIROC-ESM-CHEM		128 × 64L80
MPI-ESM-LR**	Max-Planck-Institute für Meteorologie (Max Planck Institute for Meteorology), Germany	192 × 96L47
MPI-ESM-MR**		192 × 96L95
MRI-CGCM3	Meteorological Research Institute, Japan	320 × 160L48
NorESM1-M	Norwegian Climate Centre, Norway	144 × 96L26
NorESM1-ME*		

details of experiment names and SST boundary conditions are summarized in Table 2. To reduce uncertainties, each set of experiments is integrated 30 years. The differences between sensitivity runs and control run (hereafter denoted as SST_HSM-CAM4_Clim, SST_HSM_1EWP-CAM4_Clim, SST_HSM_2EWP-CAM4_Clim, and SST_HSM_4EWP-CAM4_Clim) represent atmospheric response to specific SST anomalies, respectively. All the model datasets are interpolated onto the same $2.5^\circ \times 2.5^\circ$ grid before analysis.

We denote the ENSO developing year as year(0) and its decay year as year(1). Thus, the ENSO mature winter

[December–January–February (DJF)] is symbolized as D(0)JF(1), the following spring [March–April–May (MAM)] is denoted as MAM(1), and the following summer [June–July–August (JJA)] is denoted as JJA(1). We focus on the ENSO decay summer season [JJA(1)] from 1979 to 2005.

b. Methods

The anomalous NWPAC index is defined as the difference of 850-hPa zonal winds between a northern region (20° – 30° N, 110° – 140° E) and a southern region (5° – 15° N, 100° – 130° E), following Wang et al. (2001)

TABLE 2. Description of control and sensitivity experiments.

Experiment name	SST boundary condition
CAM4_Clim	Climatological SST with seasonal cycle.
SST_HSM	The SST anomalies in the tropical Indo-Pacific Ocean (20°S–20°N, 40°E–80°W) in the HSM from January to December are added on climatological SST.
SST_HSM_1EWP	The SST anomaly differences between the LSM and the HSM in the EWP (10°S–10°N, 140°E–170°W) are added on SST_HSM.
SST_HSM_2EWP	Doubled SST anomaly differences between the LSM and the HSM in the EWP (10°S–10°N, 140°E–170°W) are added on SST_HSM.
SST_HSM_4EWP	Quadrupled SST anomaly differences between the LSM and the HSM in the EWP (10°S–10°N, 140°E–170°W) are added on SST_HSM.

with a reversed sign. The boreal winter Niño-3.4 index is defined as the SST anomalies averaged over the region of 5°S–5°N and 120°–170°W to represent the ENSO variability. Although the atmospheric response to El Niño and La Niña is asymmetric in observations (Hoerling et al. 1997), the ENSO asymmetric features are underestimated in CMIP5 models (Zhang and Sun 2014). Therefore, the linear regression method used here is reasonable. In this study regressed anomalies are calculated in each model first and then are averaged across the models with equal weights, which is denoted as the multimodel ensemble mean (MME).

The equatorial oceanic Kelvin wave forcing function K_f is used to calculate the tropical ocean dynamic response to the zonal wind stress anomaly (Battisti 1988; Vimont et al. 2003). It is obtained by projecting the zonal wind stress regression map onto the meridional Kelvin wave structure (see Battisti 1988 for details):

$$K_f(x, \lambda) = \int_{30S}^{30N} \tau_x(x, y, \lambda) \psi_0(y) dy.$$

Here x is the longitude, y is the latitude, $\tau(x, y, \lambda)$ represents the zonal wind stress anomaly at a given lag time λ , and $\psi_0(y)$ is the meridional equatorial Kelvin wave structure. The meridional structure of equatorial Kelvin wave can be obtained through solving the dynamic equations of the upper-layer ocean on an equatorial β plane (Gill 1980; Battisti 1988). Results are generally insensitive to realistic values for the equivalent depth of the first baroclinic mode (Vimont et al. 2003). The Kelvin wave forcing function K_f indicates the relative strength of the equatorial Kelvin wave forcing produced by a given zonal wind stress, as a function of longitude. Positive (negative) values of K_f indicate that zonal wind anomalies force a downwelling (upwelling) equatorial oceanic Kelvin wave that tends to warm (cool) the SST.

To understand the physical processes associated with the SST anomaly evolution in CGCMs, the heat budget of the ocean mixed layer is analyzed as follows:

$$\frac{\partial T'}{\partial t} = \frac{Q'_{\text{net}}}{\rho C_p h} - \bar{u} \frac{\partial T'}{\partial x} - \bar{v} \frac{\partial T'}{\partial y} - u' \frac{\partial \bar{T}}{\partial x} - v' \frac{\partial \bar{T}}{\partial y} - \text{Re}'_w,$$

where T' is SST anomaly, $\rho C_p h$ is the heat capacity of the mixed layer, the mixed layer depth is determined by a temperature difference of 0.5°C between local temperature and local SST (Monterey and Levitus 1997). The net surface heat flux into the ocean is $Q_{\text{net}} = Q_{\text{SW}} + Q_{\text{LW}} - Q_{\text{LHF}} - Q_{\text{SHF}}$, where Q_{SW} , Q_{LW} , Q_{LHF} , and Q_{SHF} denote net SW radiation, net LW radiation (positive downward), LHF and SHF at the surface (positive upward), respectively. The remaining five terms are the ocean heat transport effect, including anomalous advection of mean temperature gradient and the advection of anomalous temperature gradient by mean current. As the vertical ocean current velocity is unavailable from CMIP5 model outputs, we estimate the anomalous entrainment and vertical diffusion Re'_w by surface wind anomalies over the equator qualitatively. The nonlinear advection terms are usually small and are not shown.

3. The relationship between ENSO and NWPSM simulated by CMIP5 CGCMs

ENSO is a primary factor to impact the NWP summertime climate (Huang and Wu 1989; Chang et al. 2000; Chou et al. 2003; Lin and Lu 2009; Chen and Zhou 2014). The primary climate effect of ENSO is represented in terms of precipitation and large-scale atmospheric circulation change (Bellenger et al. 2014). To evaluate the model performance in the simulation of ENSO teleconnection to the NWP summer climate in 37 state-of-the-art CGCMs during El Niño decay summers, Figs. 1a,b show the regressed anomalies of JJA(1) precipitation and 850-hPa wind on D(0)JF(1) Niño-3.4 index in observations and CGCMs MME.

In observations, the most obvious climate feature associated with ENSO is a tripole rainfall anomaly pattern accompanied by an anomalous anticyclone and an anomalous cyclone (Fig. 1a). Positive rainfall anomalies emerge over the mei-yu-baiu region (28°–38°N, 105°–150°E) and the

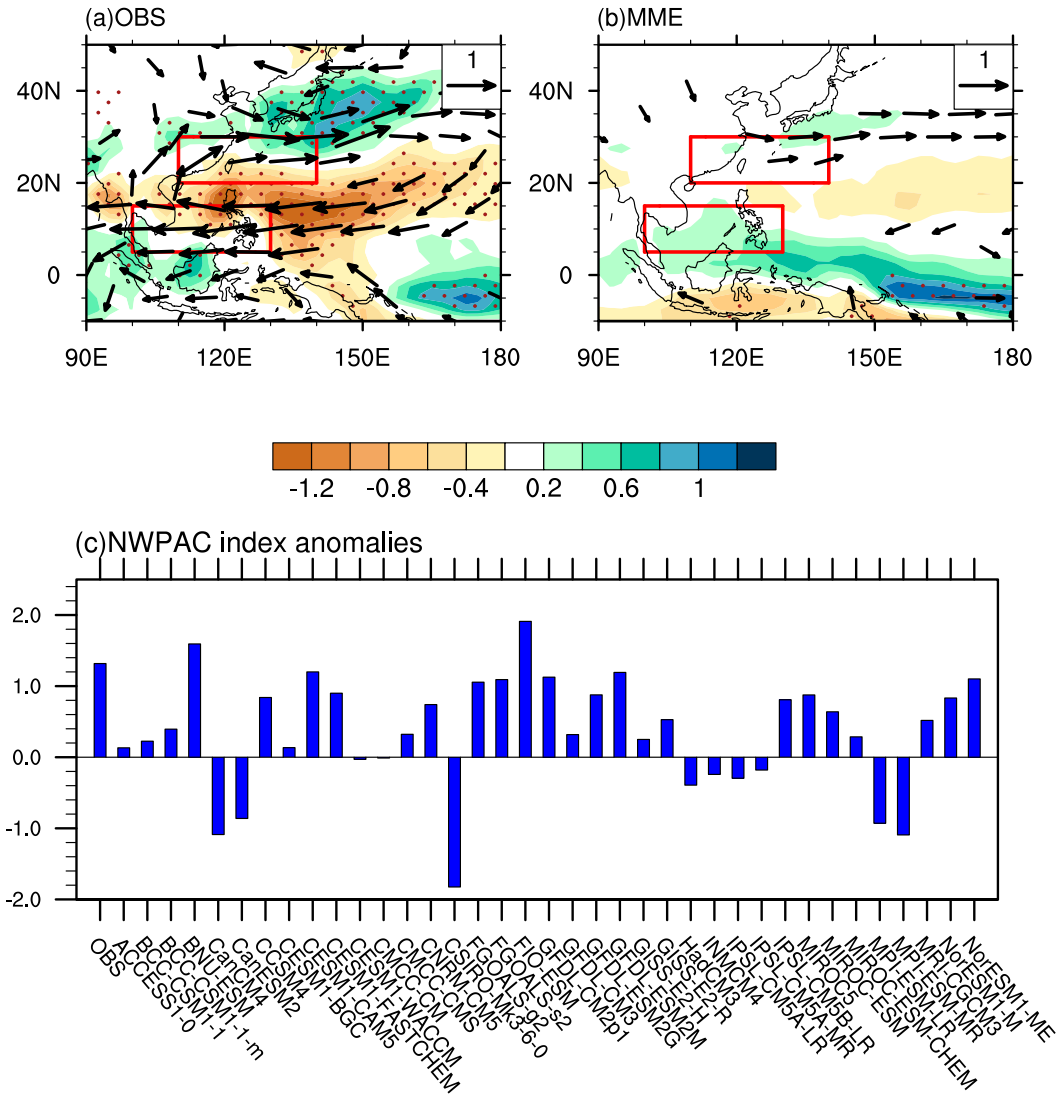


FIG. 1. Regressed anomalies of JJA(1) precipitation (shading; units: mm day^{-1}) and 850-hPa wind (vectors; units: m s^{-1}) upon the D(0)JF(1) Niño-3.4 index in (a) observations and (b) MME. (c) ENSO regressed NWPAC indices in observations and 37 CGCMs. Brown dots indicate that the regressed precipitation anomalies are significant at the 90% confidence level. Arrows are drawn if the regressed wind anomalies are significant at the 80% confidence level. Red boxes indicate the regions used to define the NWPAC index.

EWP, and negative rainfall anomalies are located in the tropical NWP. An anomalous anticyclone is located to the south of 30°N and an anomalous cyclone is located to the north of 30°N . Compared with observations, the NWPAC and rainfall anomalies are quite weak in MME. Most circulation and precipitation signals are below the 90% confidence level. Figure 1c shows the regression of JJA(1) NWPAC index on D(0)JF(1) Niño-3.4 index in observations and the 37 CGCMs. The NWPAC index anomalies spread widely among the CGCMs. In the BNU-ESM and the FIO-ESM, the NWPAC index anomalies are larger than the observations. In the other models, the NWPAC index

anomalies are smaller than the observations, and even negative NWPAC index anomalies appear in 11 models. In general, CMIP5 CGCMs show large spread in simulating the relationship of ENSO and the NWP summer climate.

4. The source of ENSO-related NWP summer climate biases in CGCMs

In this section, we investigate the source of ENSO-related NWP summer climate biases in the models. We first compare the temporal evolution of ENSO-related SST anomaly pattern between models and observations.

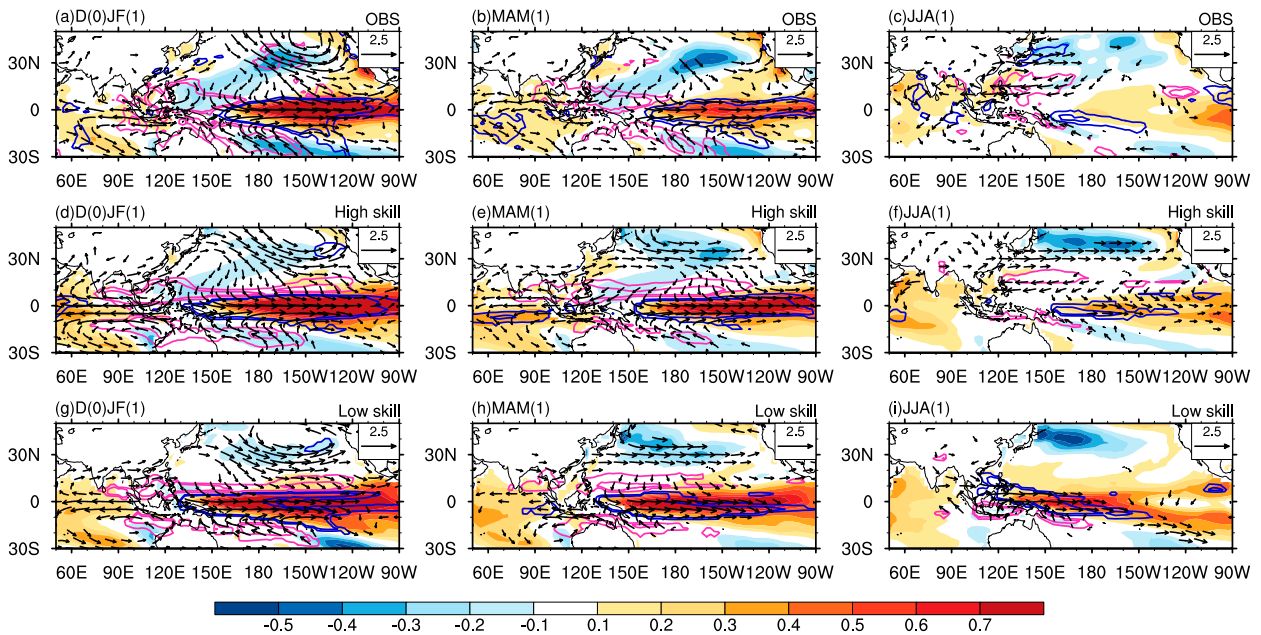


FIG. 2. Regressed anomalies of SST (shading; units: K), precipitation (contours; units: mm day^{-1}) and 850-hPa winds (vectors; units: m s^{-1}) in (left) concurrent winter [D(0)JF(1)], (center) subsequent spring [MAM(1)], and (right) subsequent summer [JJA(1)] upon the D(0)JF(1) Niño-3.4 index in (a)–(c) the observations, (d)–(f) the HSM, and (g)–(i) the LSM. Blue (pink) lines denote +0.5 and +1 (–0.5 and –1) mm day^{-1} contours of precipitation anomalies that are significant at the 90% confidence level. Arrows are drawn if the regressed wind anomalies are significant at the 90% confidence level.

Then, we document the local air–sea interaction and the Indian Ocean capacitor effect in the models compared with observations. Last, the impacts of the EWP SST anomaly bias in the model simulations are analyzed.

a. The evolution of ENSO-related SST pattern

Based on NWPAC index anomalies (Fig. 1c), two groups of models have been selected. One group has

eight models with the largest NWPAC index anomalies that are denoted by an asterisk in Table 1 and referred to as a high-skill group. The other group has eight models with obviously negative NWPAC index anomalies that are denoted by two asterisks in Table 1 and referred to as a low-skill group. We attempt to find out where the bias comes from by comparing the differences among observations and these two groups of models. Figure 2

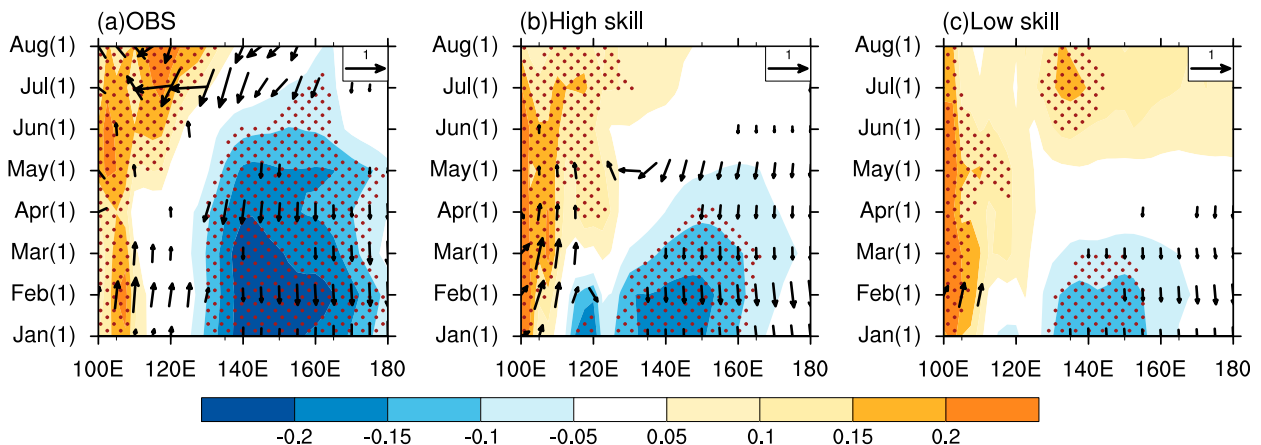


FIG. 3. Regressed anomalies of meridional-mean (5° – 20° N) 850-hPa winds (vectors; units: m s^{-1}) and SST (shading; units: K) upon the D(0)JF(1) Niño-3.4 index in (a) the observations, (b) the HSM, and (c) the LSM as a function of calendar month and longitude. Brown dots indicate that the regressed SST anomalies are significant at the 90% confidence level. Arrows are drawn if the regressed wind anomalies are significant at the 90% confidence level.

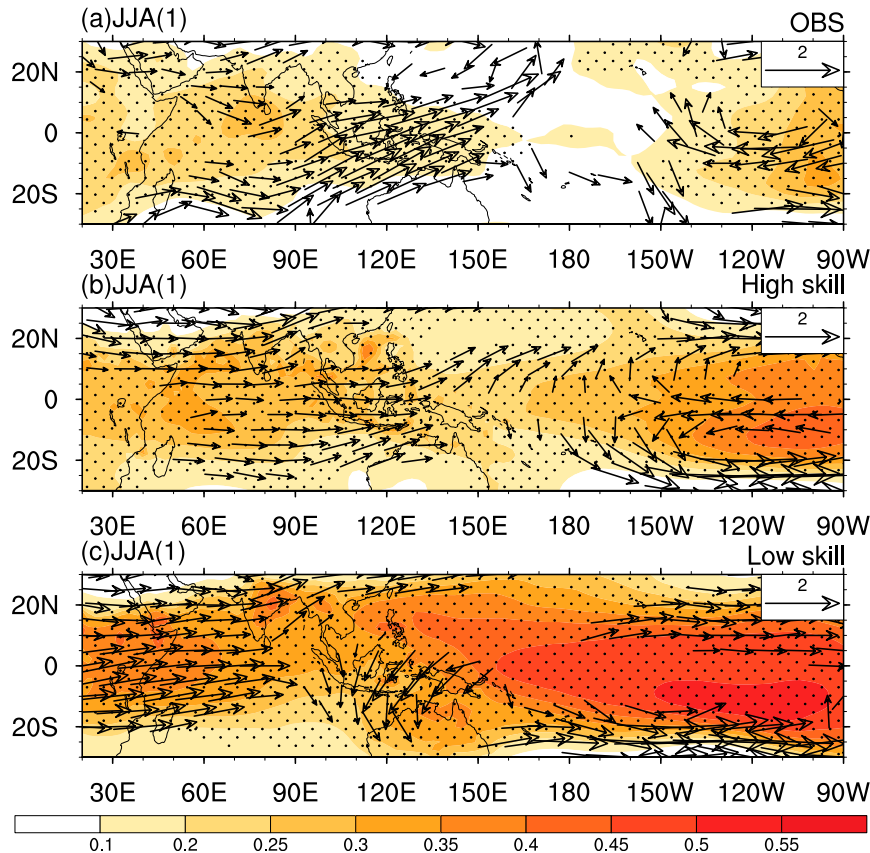


FIG. 4. Regressed anomalies of tropospheric (1000–200 hPa) temperature (shading; units: K) and 200-hPa winds (vectors; units: m s^{-1}) in JJA(1) onto the D(0)JF(1) Niño-3.4 index in (a) the observations, (b) the HSM, and (c) the LSM. Black dots indicate that the regressed temperature anomalies are significant at the 90% confidence level. Arrows are drawn if the regressed wind anomalies are significant at the 90% confidence level.

shows the evolution of SST, precipitation, and low-level circulation anomalies associated with ENSO in the observations, the MME of high-skill models (HSM), and the MME of low-skill models (LSM).

During the winter of El Niño mature phase, the ENSO-related SST extends too far west in the HSM and the LSM (Figs. 2a,d,g). This suggests an SST anomaly bias with excessive westward extension in CGCMs, which has been mentioned in previous studies (Collins et al. 2010; Kim and Yu 2012; Chowdary et al. 2014; Gong et al. 2015; Chowdary et al. 2016; Tao et al. 2016). Comparing the two group models, we find that the SST anomaly bias is more westward in the LSM than in the HSM, corresponding with more westward extension of equatorial positive rainfall anomalies and wind anomalies. As the simulation skill of ENSO-related SST pattern is better in the HSM than in the LSM, the ENSO-related atmospheric circulation anomalies in the HSM are more similar to observations. There is an anomalous anticyclone over the SCS in the HSM, while

the anomalous circulation is obviously underestimated in the LSM.

During the post-El Niño spring and summer, the observed EWP SST anomalies gradually dissipate, and an anomalous NWPAC shifts northward (Figs. 2b,c), consistent with Wu et al. (2003). In the HSM, the models reasonably reproduce the evolution of anomalous SST, rainfall, and atmospheric circulation from winter to summer (Figs. 2e,f), with gradual decay of warm SST anomalies in the EWP, SST warming in the TIO, and development of an anticyclone over the NWP. In the LSM, the ENSO-related SST anomaly decay pace displays a prominent discrepancy from the observations. The most significant SST anomaly discrepancy is that the warm EWP SST anomalies do not completely decay but persist into summer (Fig. 2i). In response to the warm SST anomaly bias in the EWP, there are above-normal precipitation and westerly wind anomalies over the western Pacific and the Maritime Continent, which are not favorable for the development of an anticyclone

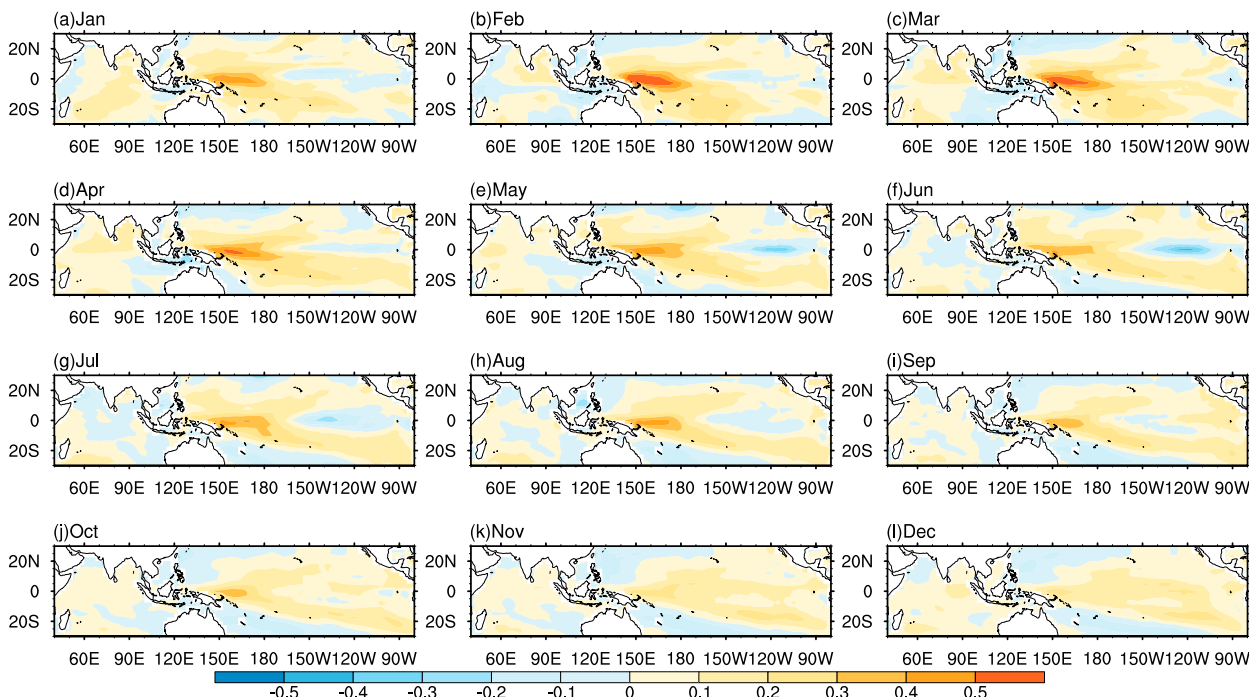


FIG. 5. Difference of regressed SST anomalies (units: K) between the LSM and HSM from January(1) to December(1).

over the NWP. As a consequence, the anomalous NWPAC is almost invisible. By comparing the differences of SST anomalies, precipitation, and low-level circulation anomalies among the observations, the HSM, and the LSM, presumably, two preliminary conclusions could be drawn as follows. One is that the criterion of choosing high-skill and low-skill models is reasonable, and the other is that the NWPAC bias might be traced back to the atmospheric response to unrealistic warm SST anomalies in the EWP, and the simulation skill of ENSO–NWP teleconnection may depend on the ENSO decay pace. The second result is consistent with [Hu and Wu \(2015\)](#), who identified overly strong impacts of EWP SST anomalies during April(1)–June(1) in CanCM4, CanESM2, CSIRO Mk3.6.0, HadCM3, INM-CM4.0, IPSL-CM5A-LR, IPSL-CM5A-MR, and MIROC5, among the 23 models in their analysis.

b. Local air–sea interaction and Indian Ocean capacitor effect

It is well documented that the formation and maintenance of NWPAC depend on the local air–sea interaction associated with ENSO teleconnection ([Wang et al. 2000, 2003](#); [Zhang and Sun 2014](#)) and ENSO-induced Indian Ocean capacitor effect ([Yang et al. 2007](#); [Xie et al. 2009](#); [Huang et al. 2010](#); [Xie et al. 2010](#); [Yang et al. 2010](#); [Xie et al. 2016](#)). To get insight into the

reasons for such a large intermodel spread in modeling ENSO-induced NWP summer climate, we investigate the model performance in simulation of local air–sea interaction and Indian Ocean capacitor effect.

The local air–sea interaction mechanism is examined in [Fig. 3](#). The observed wind anomalies associated with ENSO are characterized by an anticyclonic shear over the NWP from January(1) to July(1), corresponding to positive (negative) SST anomalies to the west (east) flank of the anticyclone. It suggests the contribution of local air–sea interaction to the maintenance of the NWPAC to early summer, which is consistent with [Wu et al. \(2010\)](#). In both groups of models, such local air–sea interaction does not persist as long as that in observations. The local air–sea interaction only persists until May(1) in the HSM and is not obvious through the period in the LSM. The short existence of the local air–sea interaction may be interpreted as a reason for the slightly weak NWPAC in most models in summer ([Fig. 1c](#)). Moreover, the local air–sea interaction is much weaker in the LSM than in the HSM, suggesting that the air–sea positive feedback in the NWP is difficult to be established in the LSM, which may be further caused by local warm NWP SST anomalies from winter to summer.

During the El Niño decay summer, the Indian Ocean warming acts like a capacitor prolonging the effect of ENSO on atmospheric circulation and anomalous climate in the NWP. It is considered as the primary

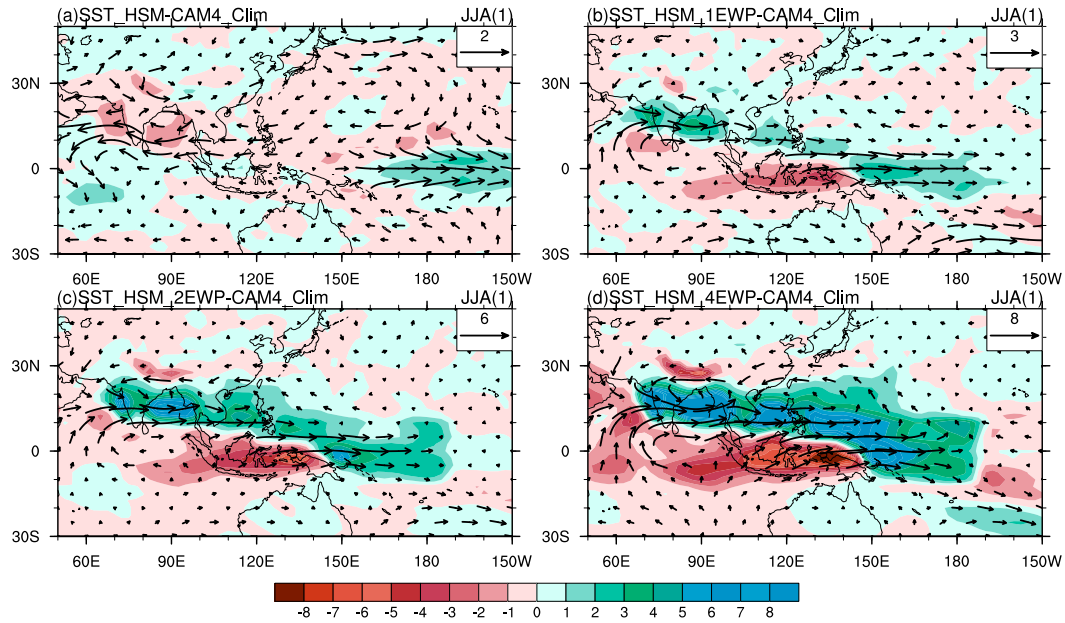


FIG. 6. Difference of 850-hPa winds (vectors; units: m s^{-1}) and precipitation (shading; units: mm day^{-1}) in JJA(1) between (a) SST_HSM, (b) SST_HSM_1EWP, (c) SST_HSM_2EWP, and (d) SST_HSM_4EWP and CAM4_Clim.

mechanism to maintain the anomalous NWPAC in summer (Yang et al. 2007; Xie et al. 2009; Huang et al. 2010; Xie et al. 2010; Yang et al. 2010; Xie et al. 2016). Chowdary et al. (2011) suggested the important role of TIO in predicting the NWP summer climate by using a CGCM. Figures 4a–c show the JJA(1) tropical tropospheric vertical mean temperature and 200-hPa wind anomalies obtained by regression onto D(0)JF(1) Niño-3.4 index in observations, the HSM, and the LSM, respectively. In observations, the tropospheric temperature presents a Matsuno–Gill pattern (Matsuno 1966; Gill 1980) anchored to the TIO with a Kelvin wave propagating into the EWP. Corresponding to the atmospheric Kelvin wave, there are strong westerly wind anomalies at upper level (Fig. 4a) and an anomalous NWPAC at low level (Fig. 1a). Since the HSM captures the ENSO-related SST anomalies during the El Niño decay summer, the Matsuno–Gill pattern of air temperature and atmospheric circulation is reproduced in the HSM (Fig. 4b). In the LSM, there are prominent warm SST anomalies in the western Pacific (Fig. 2i), which leads to positive rainfall anomalies in the EWP and triggers a Matsuno–Gill pattern over the western Pacific. Note that the Matsuno–Gill pattern is located over the TIO in the observations and the HSM but over the western Pacific in the LSM. Thus, there are low-level easterly winds anomalies over the EWP and the Maritime Continent corresponding to the Kelvin wave in the observations and the HSM (Figs. 2c,f), but there are

low-level westerly winds there in the LSM (Fig. 2i). As a consequence, the circulation anomalies in the LSM are significantly different from those in the HSM and the observations. The results show that the HSM reasonably captures the SST anomaly evolution associated with ENSO and the Indian Ocean capacitor effect, while there is significant warm SST anomaly bias in the EWP in the LSM compared with the observations, leading to unreal positive precipitation anomalies and westerly wind anomalies over the EWP and the Maritime Continent. Chowdary et al. (2016) also found a weak TIO response due to the slow decay of El Niño in a coupled model.

c. The effect of unrealistic EWP SST anomalies

To further substantiate that the source of bias is forced by the unrealistic EWP SST anomalies, we design five sets of sensitivity experiments using CAM4 (Table 2). In SST_HSM, the SST anomalies in the tropical Indian Ocean and Pacific (20°S – 20°N , 40°E – 80°W) in the HSM are added to the climatological SST from January(1) to December(1). Because the SST anomaly differences D_{sst} between the LSM and the HSM are most prominent in the EWP region (10°S – 10°N , 140°E – 170°W) throughout the entire decay year (Fig. 5), the D_{sst} in the EWP are added to the prescribed SST in SST_HSM run (i.e., SST_HSM_1EWP). We also conduct experiments with doubled and quadrupled D_{sst} in the EWP (viz., SST_HSM_2EWP and

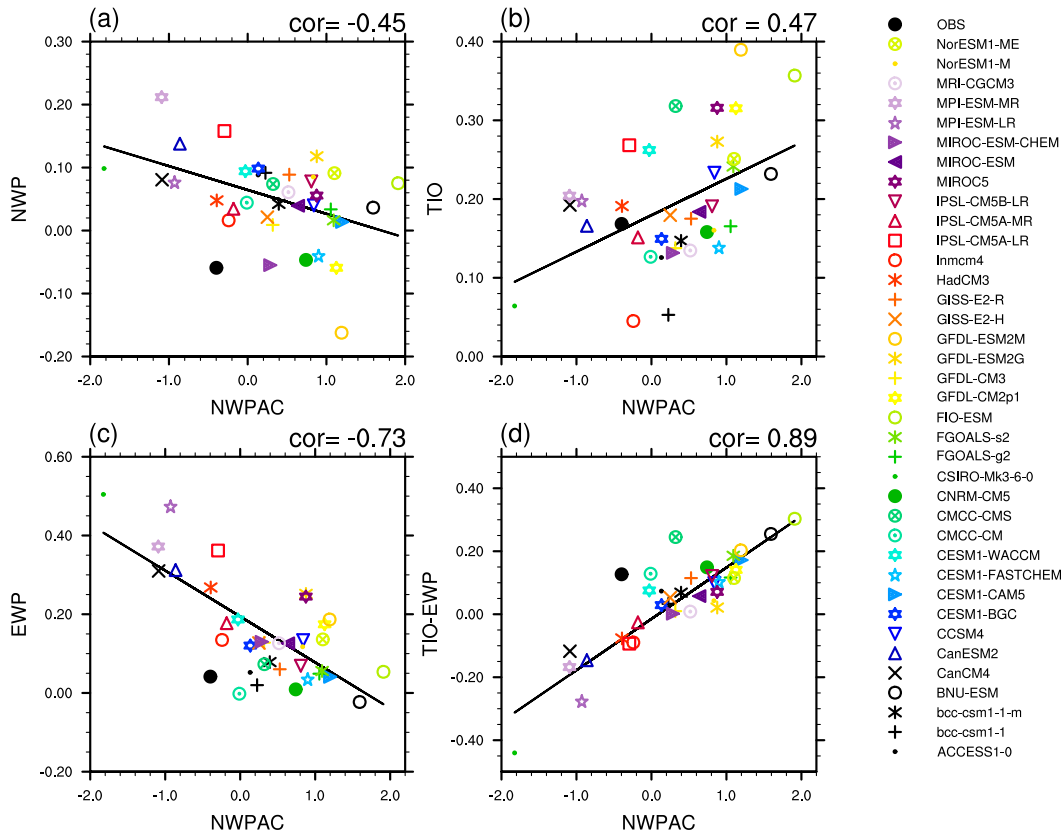


FIG. 7. Scatterplots of the JJA(1) NWPAC indices vs (a) NWP, (b) TIO, (c) EWP, and (d) TIO–EWP in 37 CMIIP5 models. Unit used is nondimensional. Black lines denote linear fit.

SST_HSM_4EWP, respectively). The artificially amplified tropical western Pacific SST anomaly differences in these experiments are to examine how the NWP circulation responds to the changing magnitude of the warming bias in the EWP in the LSM.

Figure 6 presents anomalous precipitation and 850-hPa winds in JJA(1) in four sensitivity experiments. In SST_HSM–CAM4_Clim (Fig. 6a), the low-level atmospheric circulation highly resembles that in the observations. This indicates that the atmospheric response to anomalous tropical SST could be reasonably reproduced in CAM4. In SST_HSM_1EWP–CAM4_Clim (Fig. 6b), the evolution of atmospheric circulation is quite similar to that in the LSM in Fig. 2. Significant westerly wind anomalies dominate over the tropical Indo–western Pacific, and positive tropical rainfall anomaly belt is so strong that it extends to the Indian Peninsula. Furthermore, two anomalous cyclones emerge over the SCS and the Bay of Bengal, which are Rossby wave responses to the positive rainfall anomalies over the EWP. The anomalous NWPAC shifts eastward as a result of the interference of the anomalous cyclone. In SST_HSM_2EWP–CAM4_Clim and SST_HSM_4EWP–CAM4_Clim

(Figs. 6c,d), this phenomenon is more prominent than in SST_HSM_1EWP–CAM4_Clim. Specifically, anomalous NWPAC is missing and replaced by an anomalous cyclone over the NWP, and the anomalous cyclone in the Bay of Bengal becomes stronger and the positive tropical rainfall anomaly belt is also more conspicuous than in SST_HSM_1EWP–CAM4_Clim. Overall, the results of sensitivity experiments suggest that the NWPAC bias is indeed related to the atmospheric response to the unrealistic EWP SST anomalies in most CMIP5 CGCMs. The anomalous cyclone induced by the unrealistic EWP SST anomalies interferes with the intensity and pattern of anomalous NWPAC.

From the above, the anomalous NWPAC bias in JJA(1) is related to weak local air–sea interaction, weak TIO capacitor effect and unrealistic warm EWP SST anomalies in most CGCMs. Which one is mainly responsible for this bias? To address this question, Figs. 7a–c show scatter diagrams in which the x and y axes represent NWPAC index anomalies and NWP SST anomalies (10° – 30° N, 140° E– 180°), TIO SST anomalies (0° – 20° N, 50° – 120° E), and EWP SST anomalies

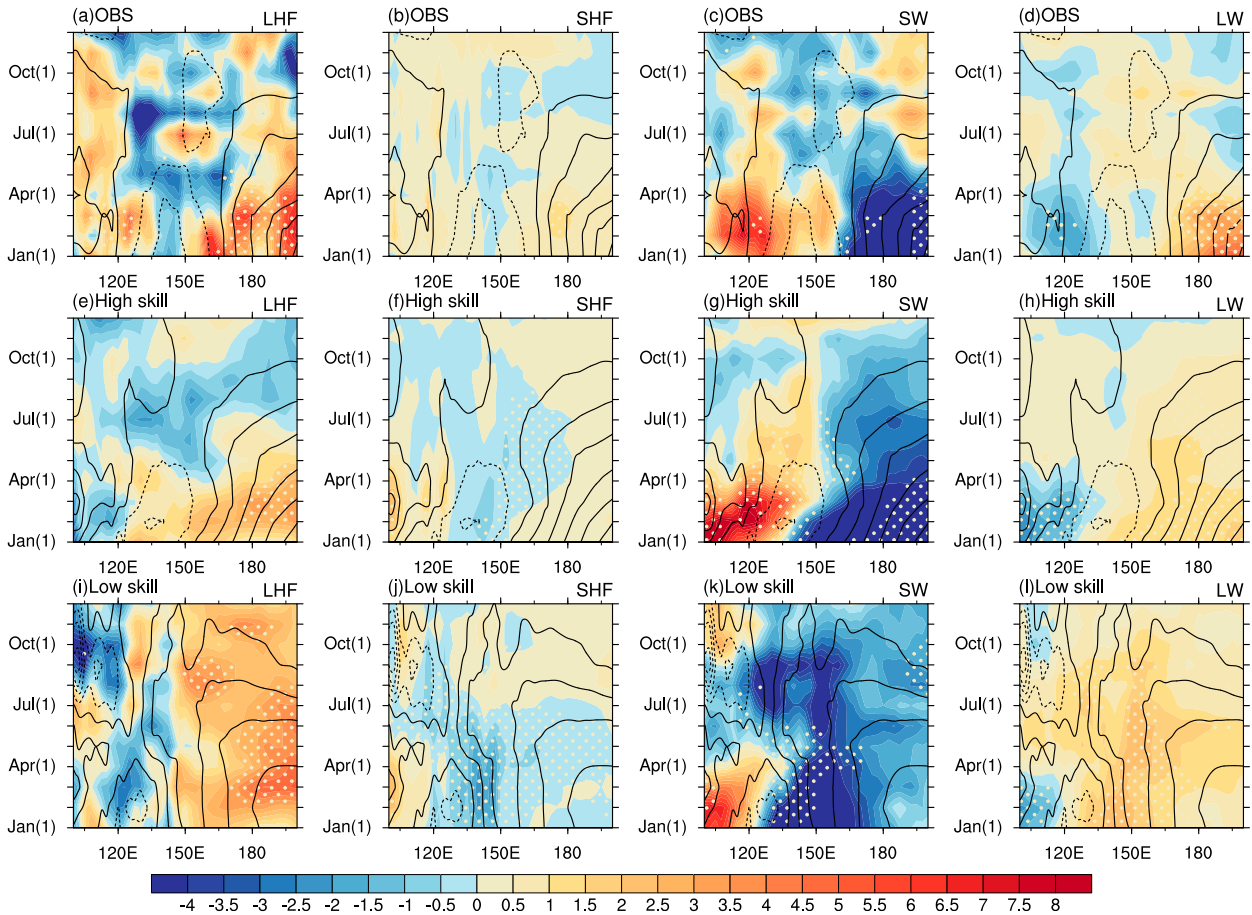


FIG. 8. Shaded anomalies of meridional-mean (10°S – 10°N) SST (contours; units: K), latent heat flux (shading; units: W m^{-2}), sensible heat flux (shading; units: W m^{-2}), shortwave radiation (shading; units: W m^{-2}), and longwave radiation (shading; units: W m^{-2}) with the D(0)JF(1) Niño-3.4 index in (a)–(d) the observations, (e)–(h) the HSM, and (i)–(l) the LSM as a function of calendar month and longitude. The signs of heat fluxes and radiations follow their conventions described in section 2b. White dots indicate that the regressed anomalies are significant at the 90% confidence level.

(10°S – 10°N , 140°E – 170°W), respectively, in 37 CMIP5 models. The correlation coefficients of NWPAC index anomalies with NWP, TIO, and EWP SST anomalies are -0.45 , 0.47 , and -0.73 , respectively, all of them exceeding the 99% confidence level. The stronger correlation between NWPAC index anomalies and EWP SST anomalies indicates that the simulated NWPAC is more sensitive to the EWP SST anomalies than to the TIO SST anomalies and the NWP SST anomalies in CGCMs. The TIO SST anomalies could generate an anomalous NWPAC by Indian Ocean capacitor effect, but the EWP SST anomalies trigger an anomalous cyclone over the NWP by a Rossby wave response. Because of the opposite effect on the NWP circulation, a new index is defined as the difference of the ENSO-related TIO SST and ENSO-related EWP SST, which is called the TIO–EWP index. Figure 7d shows the relationship between ENSO-related NWPAC index and

TIO–EWP index. The correlation coefficient between them is 0.89 , exceeding the 99% confidence level. The results of CGCMs indicate that the simulated ENSO-related NWPAC is highly related to the difference between TIO SST anomalies and EWP SST anomalies in CGCMs. Since this SST anomaly bias in the EWP provides significant effects on the ENSO–NWP relationship, what leads to the bias is another primary question to be addressed in the next section.

5. Causes of the EWP SST bias

a. Surface heat flux

To understand the physical processes of ENSO-related EWP SST anomalies, we perform a surface heat flux analysis to understand the possible causes of the warm EWP SST anomaly bias. Figure 8 shows the

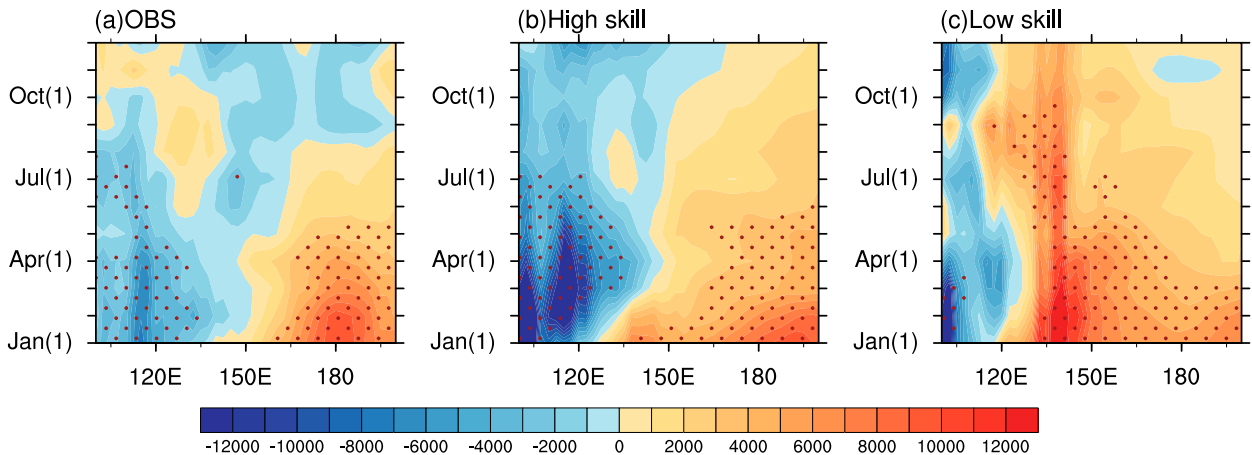


FIG. 9. Kelvin wave forcing function K_f (shading; units: N m^{-1}) anomalies from January(1) to December(1) based on regression upon the D(0)JF(1) Niño-3.4 index in (a) the observations, (b) the HSM, and (c) the LSM. Brown dots denote the regressed K_f anomalies are significant at the 90% confidence level.

evolution of ENSO-related surface heat fluxes and SST in the observations, the HSM, and the LSM. Among the four terms of heat fluxes, the patterns of LHF and SW radiation are consistent with the SST anomaly pattern and their amplitudes are larger than the others. The warm SST anomalies are accompanied by release of more LHF and gain of less SW radiation during the El Niño mature and decay phase. Thus, the LHF and SW radiation mainly serve as damping terms and are not totally balanced by LW radiation and SHF. In the LSM, there are stronger positive precipitation anomalies over the EWP in JJA(1) (Fig. 2i), and the warm EWP SST anomalies lose more LHF and obtain less SW radiation than that in observations and the HSM (Figs. 8a,c,e,j,i,k). The result suggests that surface heat flux anomalies could

not explain the warm EWP SST anomaly bias in the LSM. Hence, the main contributor to the persistence of warm EWP SST anomaly bias in the low-skill models should come from the ocean dynamic processes.

b. Ocean dynamic processes

Chowdary et al. (2014) suggested that the ocean wave adjustments and persistent westerly wind anomalies over the equatorial Pacific should be responsible for slow decay of El Niño based on the CGCM Climate Forecast System. Previous studies indicate that the zonal wind anomalies over the EWP have important influences on the ENSO cycle by triggering equatorial Kelvin waves (e.g., Zhang and Huang 1998; Huang et al. 2001). It is noteworthy that prominent easterly wind

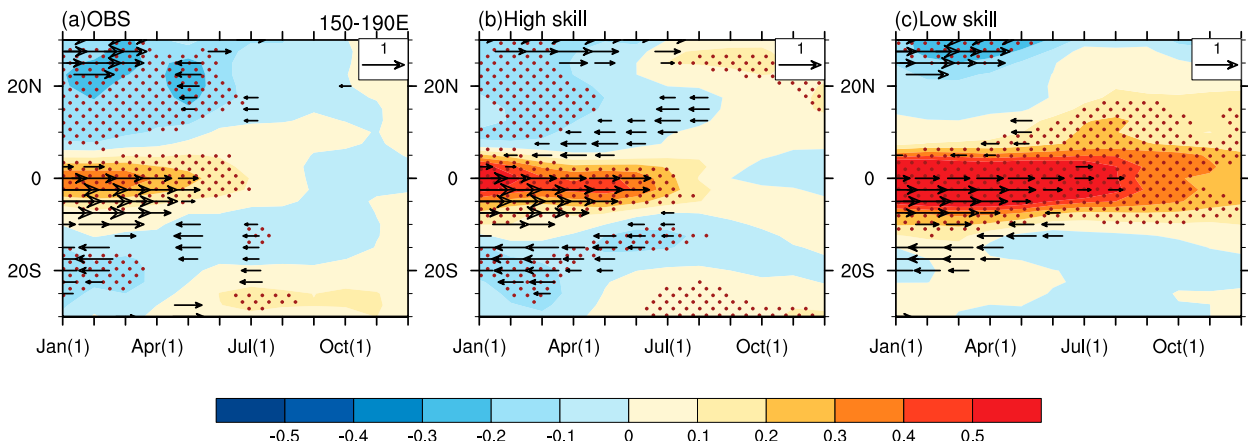


FIG. 10. Regressed anomalies of zonal-mean (150°E – 170°W) SST (shading; units: K), 1000-hPa zonal wind (vectors; units: m s^{-1}) upon the D(0)JF(1) Niño-3.4 index in (a) the observations, (b) the HSM, and (c) the LSM as a function of calendar month and latitude. Brown dots denote that the regressed SST anomalies are significant at the 90% confidence level. Arrows are drawn if the regressed zonal wind anomalies are significant at the 90% confidence level.

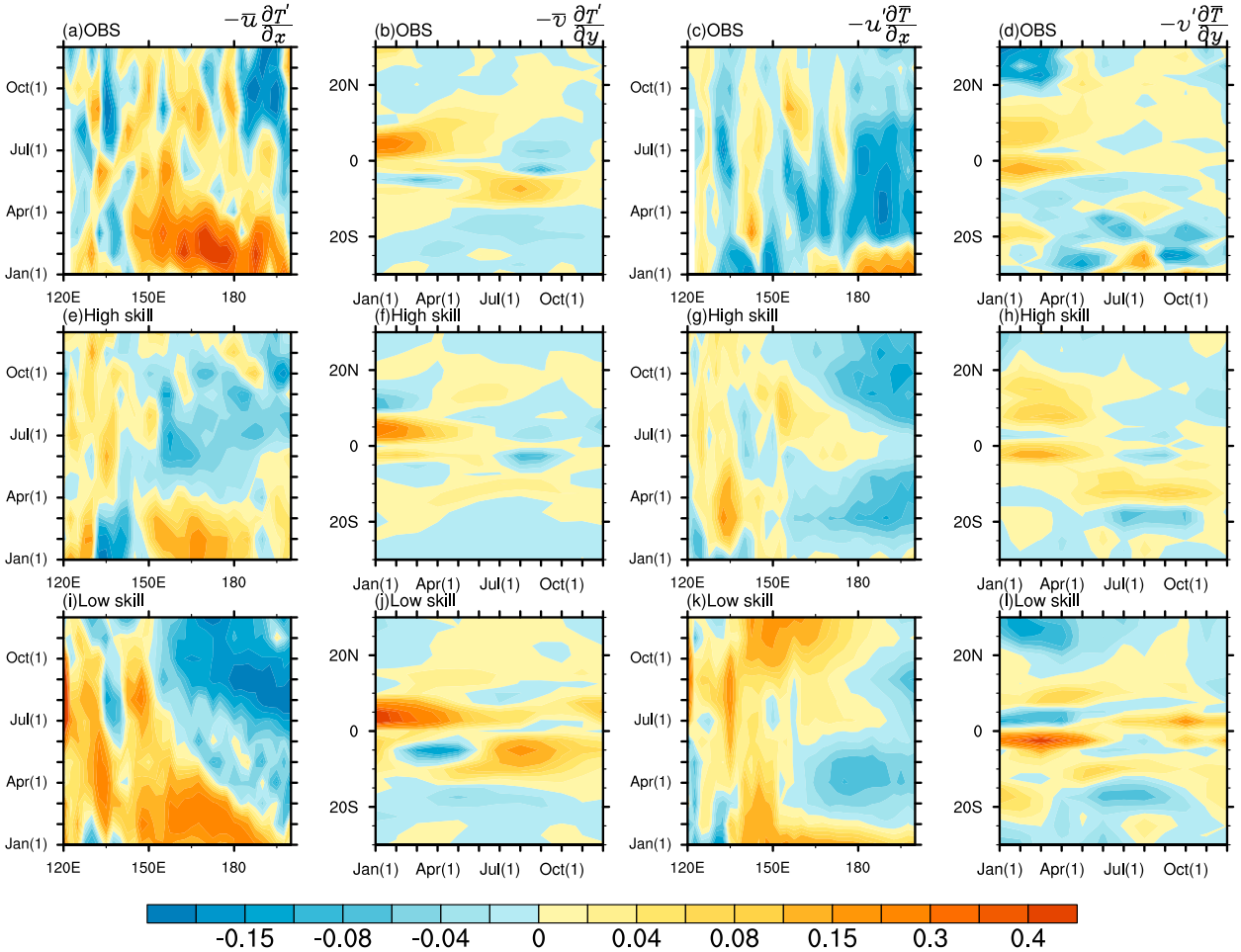


FIG. 11. (a) Vertical averages of mean zonal advection and (b) mean meridional advection of anomalous temperature gradient, (c) vertical integrations of anomalous zonal advection, and (d) anomalous meridional advection of mean temperature gradient in the mixed layer in observations, in which temperature and current anomalies are obtained by regression upon the D(0)JF(1) Niño-3.4 index. The zonal advection terms (units: $^{\circ}\text{C day}^{-1}$) are averages over 10°S – 10°N and as a function of calendar month and longitude. The meridional advection terms (units: $^{\circ}\text{C day}^{-1}$) are averages over 140°E – 170°W and as a function of calendar month and latitude. (e)–(h) As in (a)–(d), but in the HSM; (i)–(l) as in (a)–(d), but in the LSM.

anomalies always dominate the Maritime Continent and western Pacific from boreal winter to summer in the observations and the HSM (Figs. 2a–f). The easterly wind anomalies are extremely weak in boreal winter and spring and replaced by westerly wind anomalies in summer in the LSM (Figs. 2h–i), which is not conducive to upwelling equatorial Kelvin wave. The evolution of anomalous equatorial Kelvin wave forcing function K_f associated with ENSO during the El Niño decay year is shown in Fig. 9. Negative (positive) values of K_f denote upwelling (downwelling) Kelvin wave. It is clear that significant negative values of K_f appear in the tropical Indo–western Pacific in January(1) in the observations and the HSM, and then the upwelling Kelvin wave propagates eastward. However, in response to westerly wind anomalies over the EWP, there is downwelling

Kelvin wave dominating in summer in the LSM. The oceanic Kelvin wave hardly affects SST directly in the EWP owing to the deep thermocline there. However, the thermocline in the equatorial eastern Pacific could be affected and the SST there could be modulated. In turn, the zonal SST gradient and wind along the equatorial Pacific could be altered, which may change the SST in the EWP indirectly.

Furthermore, Fig. 10 shows the evolution of zonal-mean (150°E – 170°W) SST anomalies and surface zonal wind anomalies during the El Niño decay year. Note that there are obvious westerly wind anomalies on the equator from January(1) to June(1) in observations and the HSM (Figs. 10a,b), which is conducive to downwelling and warming of SST. The westerly wind anomalies decline quickly in the following summer, which

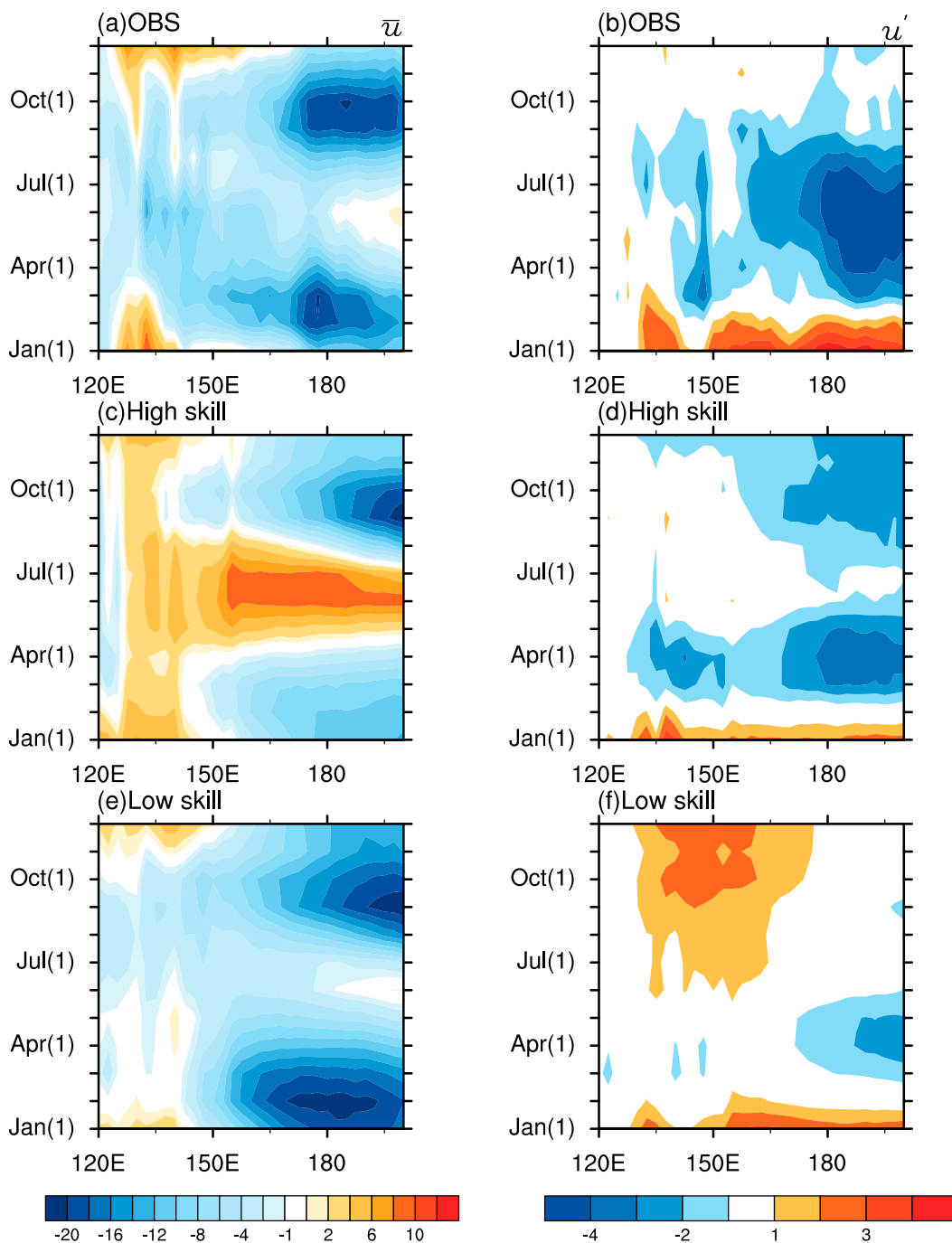


FIG. 12. (a) Vertical averages of monthly climatology of zonal current and (b) regressed zonal current anomalies (units: m day^{-1}) upon the $D(0)JF(1)$ Niño-3.4 index in the mixed layer in the observations. These are averages over 10°S – 10°N and as a function of calendar month and longitude. (c),(d) As in (a),(b), but in the HSM; (e),(f) as in (c),(d), but in the LSM.

could be attributed to the generation of easterly wind anomalies induced by the Indian Ocean capacitor effect in JJA(1). Thus, the SST anomalies decline in the observations and the HSM in JJA(1). Meanwhile, in the LSM, owing to the persistence of warm EWP SST

anomalies and associated Rossby wave response (Matsuno 1966; Gill 1980), prominent westerly wind anomalies persist into boreal summer and autumn (Fig. 10c), inducing downwelling and warming of SST in the EWP. Indeed, persistent westerly wind anomalies

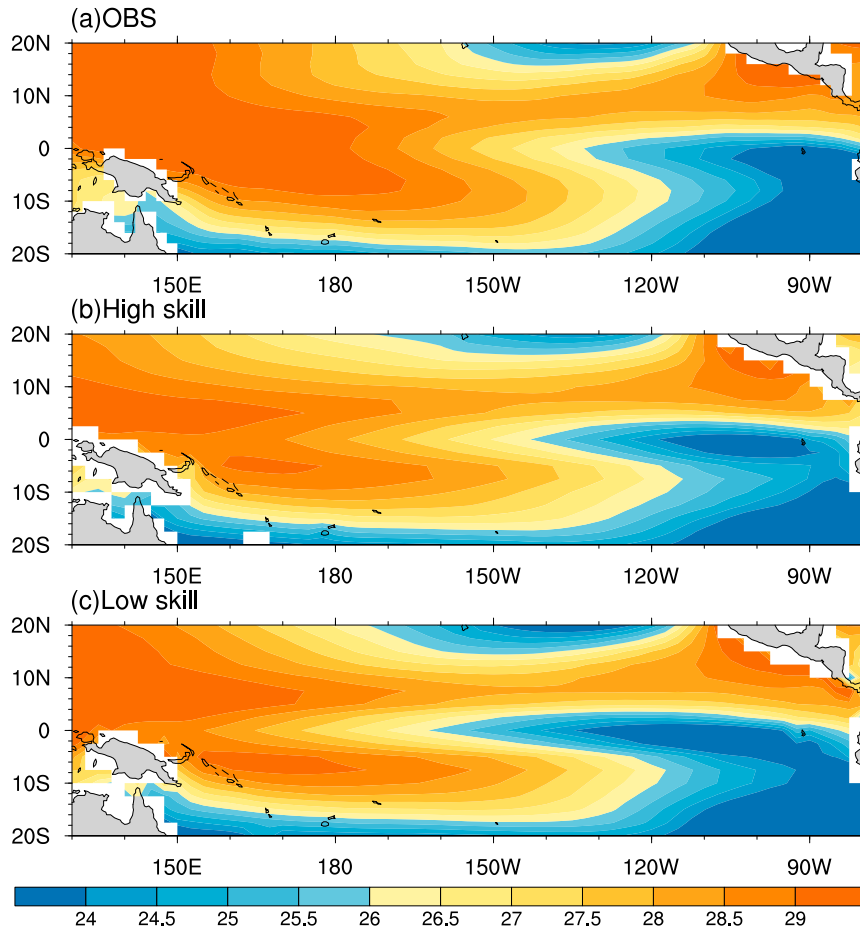


FIG. 13. Summer mean climatology of SST (units: °C) in the tropical Pacific in (a) the observations, (b) the HSM, and (c) the LSM.

over the equatorial Pacific can affect the decay of El Niño, which is consistent with Chowdary et al. (2014).

We perform an ocean heat budget analysis of the ocean mixed layer to understand the contribution of oceanic advection. The mean current advection of anomalous temperature gradient (hereafter referred to as mean advection) and the anomalous current advection of mean temperature gradient (hereafter referred to as anomalous advection) in the observations, the HSM, and the LSM are shown in Fig. 11. We focus on the change of EWP SST anomalies (10°S–10°N, 140°E–170°W) in JJA(1). Compared with observations, there is significant cooling due to mean zonal advection $-\bar{u}(\partial T'/\partial x)$ from April(1) in the HSM, which may be attributed to unreal mean zonal current (Fig. 12c), facilitating the decay of El Niño (Fig. 11e). Meanwhile, warm zonal advectons $[-\bar{u}(\partial T'/\partial x)$ and $-u'(\partial \bar{T}/\partial x)$] are stronger around 150°E in the LSM than in the HSM from winter to summer, which also contribute to the warm bias in the EWP in the LSM.

Further analysis is conducted to examine the respective contributions of current and SST gradient to the oceanic advection in the LSM. From Fig. 13, the excessive cold tongue bias is prominent in CMIP5 CGCMs, which is consistent with previous studies (Li and Xie 2014; Li et al. 2015, 2016). The cold tongue extends more westward in the LSM than the HSM and the observation, leading to larger west-minus-east mean zonal SST gradient $\partial \bar{T}/\partial x$ in the EWP (Fig. 14f). In addition, there are prominent anomalous easterly current u' (Fig. 12f) and anomalous zonal temperature gradient $\partial T'/\partial x$ (Fig. 14e) associated with the westward extension of ENSO-related SST pattern around 150°E in the LSM during the post-ENSO summer, which contribute to the warm SST anomaly bias in the EWP. In general, the ENSO-related SST pattern extends westward during the El Niño mature phase and strengthens the westerly wind anomalies over the Indo-western Pacific. The excessive cold tongue causes larger west-minus-east mean zonal SST gradient in the EWP in the LSM

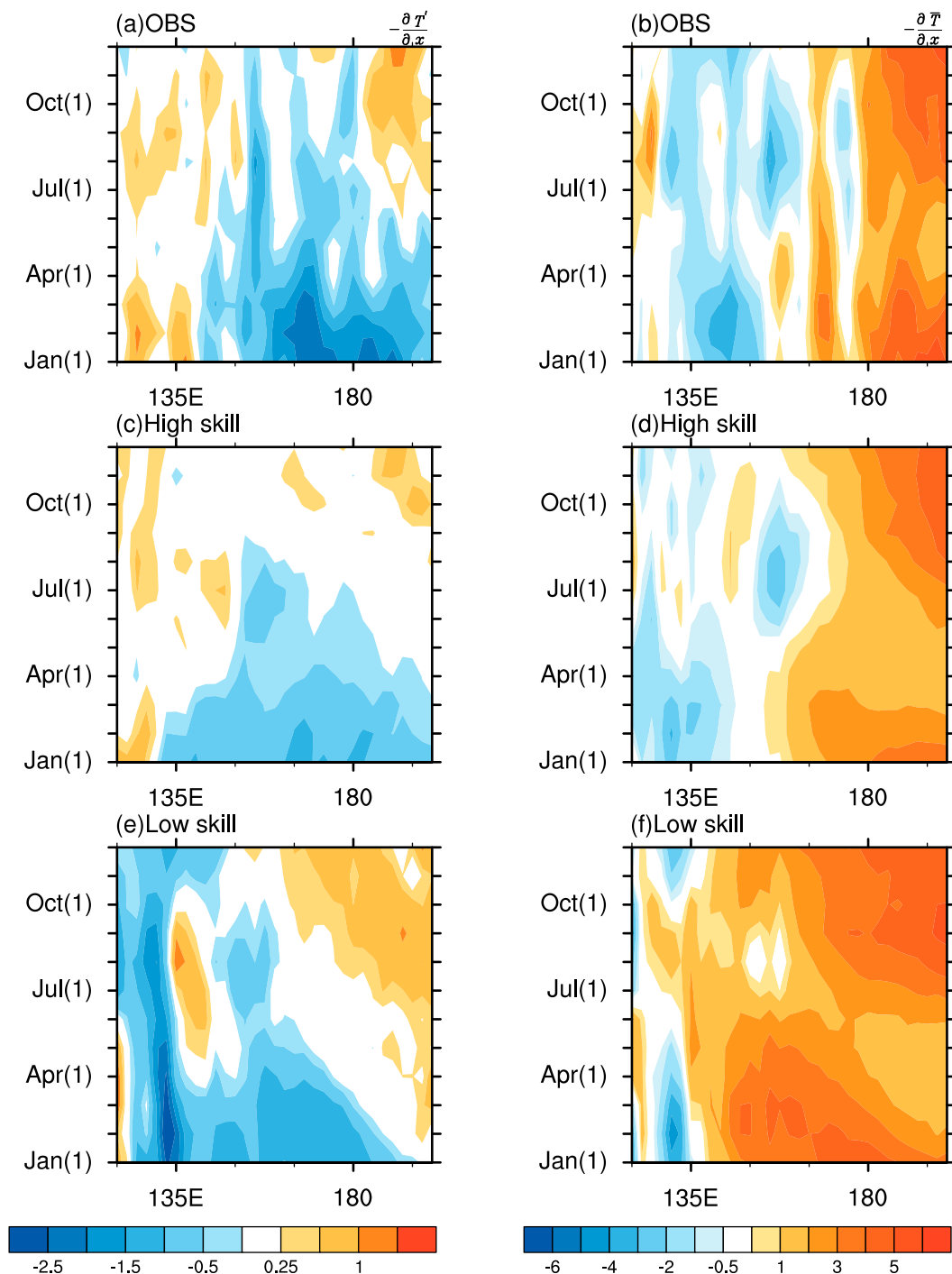


FIG. 14. (a) Vertical averages of anomalous zonal temperature gradient and (b) mean zonal temperature gradient [units: $^{\circ}\text{C m}^{-1} (86\,400)^{-1}$] in the mixed layer in the observations, in which anomalous temperature and current velocities are obtained by regression upon the D(0)JF(1) Niño-3.4 index. These are averages over 10°S – 10°N and as a function of calendar month and longitude. (c),(d) As in (a),(b), but in the HSM; (e),(f) as in (a),(b), but in the LSM.

than in observations and the HSM. The resultant anomalous warm advection leads to persistence of the warm SST anomalies in the EWP during the following spring and summer and causes the slow decay of

El Niño in the LSM. In turn, the warm SST anomaly bias in the EWP strengthens the westerly wind anomalies by triggering local convection and atmospheric Rossby wave.

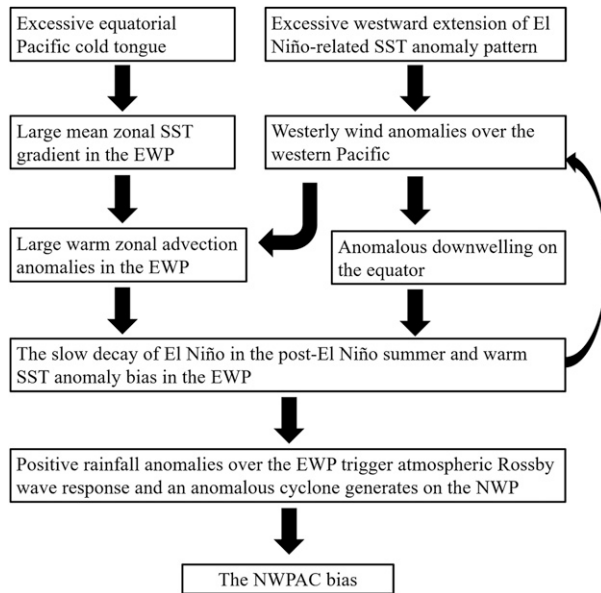


FIG. 15. Schematic diagram illustrating the processes for the NWPAC bias during the El Niño decay summer in CMIP5 CGCMs.

6. Summary

In this study, we investigate plausible reasons for biases in simulation of the ENSO–NWP teleconnection in most CMIP5 CGCMs, including weaker NWPAC anomalies and excessive westward extension of positive rainfall anomalies in the EWP. The possible reasons for and processes leading to these biases are displayed in Fig. 15. Major conclusions are summarized as follows.

By comparing the evolution of ENSO-related SST anomaly pattern, the local air–sea interaction, and the Indian Ocean capacitor effect among the observations and high-skill and low-skill models, we find that the biases of the ENSO-related NWP summer climate could be mainly attributed to the simulation of ENSO decay pace. The unrealistic EWP SST anomalies persist into the ENSO decay summer, which generate above-normal precipitation over the EWP and an anomalous cyclone over the NWP. In turn, the anomalous cyclone could modify the intensity and position of anomalous NWPAC induced by the Indian Ocean capacitor effect. This conclusion is confirmed by sensitivity experiments with CAM4.

A new index–TIO–EWP index is defined as the difference of ENSO-related SST between TIO and EWP, which has a close relationship with the anomalous NWPAC. Those models with a TIO–EWP index close to observations could simulate ENSO–NWP teleconnection well, which will be useful for the selection of reasonable models in predicting the summer climate of East Asia and NWP.

The occurrence of the SST anomaly bias in the EWP may involve a positive air–sea feedback. On one hand, the excessive climatological cold tongue increases climatological zonal SST gradient $\partial\bar{T}/\partial x$ in the EWP. Because of the westerly wind anomalies over the western Pacific induced by the warm SST anomaly bias in the LSM, the larger climatological zonal SST gradient $\partial\bar{T}/\partial x$ could lead to warmer zonal advectations $-u'\partial\bar{T}/\partial x$, which could favor the persistence of the warm EWP SST anomaly in the LSM. In addition, the downwelling on the equator forced by westerly wind anomalies may also contribute to the persistence of EWP SST anomaly bias. On the other hand, the warm EWP SST anomaly bias could strengthen westerly wind anomalies over the western Pacific by triggering convection and atmospheric Rossby wave, which, in turn, could increase the warm SST anomaly bias in the EWP.

This study suggests that the model needs to produce a reasonable decay pace of ENSO in the equatorial Pacific to obtain proper ENSO–NWP teleconnection, and mean state SST bias may be responsible for the bias of the evolution of ENSO. Here, we only point out the main and common biases about ENSO-induced NWP summer climate in CMIP5 CGCMs. There may be some other biases in individual models, which need to be explored. Further understanding of the biases may contribute to improvement of the prediction skill of ENSO teleconnection.

Acknowledgments. We thank the anonymous reviewers for the valuable comments that helped us to improve the manuscript. We acknowledge the World Climate Research Programme’s Working Group on Coupled Modelling, which is responsible for CMIP, and we thank the climate modeling groups listed in Table 1 for producing and making available their model output. For CMIP the U.S. Department of Energy’s Program for Climate Model Diagnosis and Intercomparison provides coordinating support and led development of software infrastructure in partnership with the Global Organization for Earth System Science Portals. This work was supported by the National Natural Science Foundation of China (91337105, 41425019, and 41275083) and the public science and technology research funds projects of ocean (201505013).

REFERENCES

- Adler, R. F., and Coauthors, 2003: The Version-2 Global Precipitation Climatology Project (GPCP) monthly precipitation analysis (1979–present). *J. Hydrometeorol.*, **4**, 1147–1167, doi:10.1175/1525-7541(2003)004<1147:TVGPCP>2.0.CO;2.
- Battisti, D. S., 1988: Dynamics and thermodynamics of a warming event in a coupled tropical atmosphere ocean model. *J. Atmos. Sci.*, **45**, 2889–2919, doi:10.1175/1520-0469(1988)045<2889:DATOAW>2.0.CO;2.
- Bellenger, H., E. Guilyardi, J. Leloup, M. Lengaigne, and J. Vialard, 2014: ENSO representation in climate models:

- From CMIP3 to CMIP5. *Climate Dyn.*, **42**, 1999–2018, doi:10.1007/s00382-013-1783-z.
- Cao, J., R. Lu, J. Hu, and H. Wang, 2013: Spring Indian Ocean–western Pacific SST contrast and the East Asian summer rainfall anomaly. *Adv. Atmos. Sci.*, **30**, 1560–1568, doi:10.1007/s00376-013-2298-6.
- Carton, J. A., and B. S. Giese, 2008: A reanalysis of ocean climate using Simple Ocean Data Assimilation (SODA). *Mon. Wea. Rev.*, **136**, 2999–3017, doi:10.1175/2007MWR1978.1.
- Chang, C. P., Y. S. Zhang, and T. Li, 2000: Interannual and interdecadal variations of the East Asian summer monsoon and tropical Pacific SSTs. Part I: Roles of the subtropical ridge. *J. Climate*, **13**, 4310–4325, doi:10.1175/1520-0442(2000)013<4310:IAIVOT>2.0.CO;2.
- Chen, W., J.-K. Park, B. Dong, R. Lu, and W.-S. Jung, 2012: The relationship between El Niño and the western North Pacific summer climate in a coupled GCM: Role of the transition of El Niño decaying phases. *J. Geophys. Res.*, **117**, D12111, doi:10.1029/2011JD017385.
- Chen, X. L., and T. J. Zhou, 2014: Relative role of tropical SST forcing in the 1990s periodicity change of the Pacific–Japan pattern interannual variability. *J. Geophys. Res. Atmos.*, **119**, 13 043–13 066, doi:10.1002/2014JD022064.
- Chou, C., J. Y. Tu, and J. Y. Yu, 2003: Interannual variability of the western North Pacific summer monsoon: Differences between ENSO and non-ENSO years. *J. Climate*, **16**, 2275–2287, doi:10.1175/2761.1.
- , L. F. Huang, J. Y. Tu, L. S. Tseng, and Y. C. Hsueh, 2009: El Niño impacts on precipitation in the western North Pacific–East Asian sector. *J. Climate*, **22**, 2039–2057, doi:10.1175/2008JCLI2649.1.
- Chowdary, J. S., S.-P. Xie, J.-J. Luo, J. Hafner, S. Behera, Y. Masumoto, and T. Yamagata, 2011: Predictability of northwest Pacific climate during summer and the role of the tropical Indian Ocean. *Climate Dyn.*, **36**, 607–621, doi:10.1007/s00382-009-0686-5.
- , A. Parekh, C. Gnanaseelan, and P. Sreenivas, 2014: Interdecadal modulation of ENSO teleconnections to the Indian Ocean in a coupled model: Special emphasis on decay phase of El Niño. *Global Planet. Change*, **112**, 33–40, doi:10.1016/j.gloplacha.2013.11.003.
- , —, R. Kakatkar, C. Gnanaseelan, G. Srinivas, P. Singh, and M. K. Roxy, 2016: Tropical Indian Ocean response to the decay phase of El Niño in a coupled model and associated changes in south and east-Asian summer monsoon circulation and rainfall. *Climate Dyn.*, **47**, 831–844, doi:10.1007/s00382-015-2874-9.
- Collins, M., and Coauthors, 2010: The impact of global warming on the tropical Pacific Ocean and El Niño. *Nat. Geosci.*, **3**, 391–397, doi:10.1038/ngeo868.
- Gill, A. E., 1980: Some simple solutions for heat-induced tropical circulation. *Quart. J. Roy. Meteor. Soc.*, **106**, 447–462, doi:10.1002/qj.49710644905.
- Gong, H., L. Wang, W. Chen, D. Nath, G. Huang, and W. Tao, 2015: Diverse influences of ENSO on the East Asian–western Pacific winter climate tied to different ENSO properties in CMIP5 models. *J. Climate*, **28**, 2187–2202, doi:10.1175/JCLI-D-14-00405.1.
- He, C., and T. J. Zhou, 2015: Responses of the western North Pacific subtropical high to global warming under RCP4.5 and RCP8.5 scenarios projected by 33 CMIP5 models: The dominance of tropical Indian Ocean–tropical western Pacific SST gradient. *J. Climate*, **28**, 365–380, doi:10.1175/JCLI-D-13-00494.1.
- Hoerling, M. P., A. Kumar, and M. Zhong, 1997: El Niño, La Niña, and the nonlinearity of their teleconnections. *J. Climate*, **10**, 1769–1786, doi:10.1175/1520-0442(1997)010<1769:ENOLNA>2.0.CO;2.
- Hu, K., G. Huang, X.-T. Zheng, S.-P. Xie, X. Qu, Y. Du, and L. Liu, 2014: Interdecadal variations in ENSO influences on north-west Pacific–East Asian early summertime climate simulated in CMIP5 models. *J. Climate*, **27**, 5982–5998, doi:10.1175/JCLI-D-13-00268.1.
- Hu, W., and R. Wu, 2015: Relationship between South China Sea precipitation variability and tropical Indo-Pacific SST anomalies in IPCC CMIP5 models during spring-to-summer transition. *Adv. Atmos. Sci.*, **32**, 1303–1318, doi:10.1007/s00376-015-4250-4.
- Huang, G., K. Hu, and S.-P. Xie, 2010: Strengthening of tropical Indian Ocean teleconnection to the northwest Pacific since the mid-1970s: An atmospheric GCM study. *J. Climate*, **23**, 5294–5304, doi:10.1175/2010JCLI3577.1.
- Huang, R., and Y. Wu, 1989: The influence of ENSO on the summer climate change in China and its mechanism. *Adv. Atmos. Sci.*, **6**, 21–32, doi:10.1007/BF02656915.
- , R. Zhang, and B. Yan, 2001: Dynamical effect of the zonal wind anomalies over the tropical western Pacific on ENSO cycles. *Sci. China*, **44D**, 1089–1098, doi:10.1007/BF02906865.
- Kalnay, E., and Coauthors, 1996: The NCEP/NCAR 40-Year Reanalysis Project. *Bull. Amer. Meteor. Soc.*, **77**, 437–471, doi:10.1175/1520-0477(1996)077<0437:TNYRP>2.0.CO;2.
- Kim, S. T., and J.-Y. Yu, 2012: The two types of ENSO in CMIP5 models. *Geophys. Res. Lett.*, **39**, L11704, doi:10.1029/2012GL052006.
- Lau, N. C., and M. J. Nath, 2000: Impact of ENSO on the variability of the Asian–Australian monsoons as simulated in GCM experiments. *J. Climate*, **13**, 4287–4309, doi:10.1175/1520-0442(2000)013<4287:IOEOTV>2.0.CO;2.
- Li, G., and S.-P. Xie, 2014: Tropical biases in CMIP5 multimodel ensemble: The excessive equatorial Pacific cold tongue and double ITCZ problems. *J. Climate*, **27**, 1765–1780, doi:10.1175/JCLI-D-13-00337.1.
- , Y. Du, H. Xu, and B. Ren, 2015: An intermodel approach to identify the source of excessive equatorial Pacific cold tongue in CMIP5 models and uncertainty in observational datasets. *J. Climate*, **28**, 7630–7640, doi:10.1175/JCLI-D-15-0168.1.
- , S.-P. Xie, Y. Du, and Y. Luo, 2016: Effects of excessive equatorial cold tongue bias on the projections of tropical Pacific climate change. Part I: The warming pattern in CMIP5 multi-model ensemble. *Climate Dyn.*, doi:10.1007/s00382-016-3043-5, in press.
- Lin, Z. D., and R. Y. Lu, 2009: The ENSO’s effect on eastern China rainfall in the following early summer. *Adv. Atmos. Sci.*, **26**, 333–342, doi:10.1007/s00376-009-0333-4.
- Matsumo, T., 1966: Quasi-geostrophic motions in the equatorial area. *J. Meteor. Soc. Japan*, **44**, 25–43.
- Monterey, G., and S. Levitus, 1997: Seasonal variability of mixed layer depth for the World Ocean. NOAA Atlas NESDIS 14, 102 pp.
- Smith, T. M., R. W. Reynolds, T. C. Peterson, and J. Lawrimore, 2008: Improvements to NOAA’s historical merged land–ocean surface temperature analysis (1880–2006). *J. Climate*, **21**, 2283–2296, doi:10.1175/2007JCLI2100.1.
- Song, F. F., and T. J. Zhou, 2014: The climatology and interannual variability of East Asian summer monsoon in CMIP5 coupled models: Does air–sea coupling improve the simulations? *J. Climate*, **27**, 8761–8777, doi:10.1175/JCLI-D-14-00396.1.

- Tao, W., G. Huang, K. Hu, H. Gong, G. Wen, and L. Liu, 2016: A study of biases in simulation of the Indian Ocean basin mode and its capacitor effect in CMIP3/CMIP5 models. *Climate Dyn.*, **46**, 205–226, doi:10.1007/s00382-015-2579-0.
- Taylor, K. E., R. J. Stouffer, and G. A. Meehl, 2012: An overview of CMIP5 and the experiment design. *Bull. Amer. Meteor. Soc.*, **93**, 485–498, doi:10.1175/BAMS-D-11-00094.1.
- Terao, T., and T. Kubota, 2005: East-west SST contrast over the tropical oceans and the post El Niño western North Pacific summer monsoon. *Geophys. Res. Lett.*, **32**, L15706, doi:10.1029/2005GL023010.
- Vimont, D. J., J. M. Wallace, and D. S. Battisti, 2003: The seasonal footprinting mechanism in the Pacific: Implications for ENSO. *J. Climate*, **16**, 2668–2675, doi:10.1175/1520-0442(2003)016<2668:TSEMIT>2.0.CO;2.
- Wang, B., R. G. Wu, and X. H. Fu, 2000: Pacific–East Asian teleconnection: How does ENSO affect East Asian climate? *J. Climate*, **13**, 1517–1536, doi:10.1175/1520-0442(2000)013<1517:PEATHD>2.0.CO;2.
- , —, and K. M. Lau, 2001: Interannual variability of the Asian summer monsoon: Contrasts between the Indian and the western North Pacific–East Asian monsoons. *J. Climate*, **14**, 4073–4090, doi:10.1175/1520-0442(2001)014<4073:IVOTAS>2.0.CO;2.
- , —, and T. Li, 2003: Atmosphere–warm ocean interaction and its impacts on Asian–Australian monsoon variation. *J. Climate*, **16**, 1195–1211, doi:10.1175/1520-0442(2003)16<1195:AOIAII>2.0.CO;2.
- Wu, B., T. Li, and T. Zhou, 2010: Relative contributions of the Indian Ocean and local SST anomalies to the maintenance of the western North Pacific anomalous anticyclone during the El Niño decaying summer. *J. Climate*, **23**, 2974–2986, doi:10.1175/2010JCLI3300.1.
- Wu, R. G., Z. Z. Hu, and B. P. Kirtman, 2003: Evolution of ENSO-related rainfall anomalies in East Asia. *J. Climate*, **16**, 3742–3758, doi:10.1175/1520-0442(2003)016<3742:EOERAI>2.0.CO;2.
- , G. Huang, Z. C. Du, and K. M. Hu, 2014: Cross-season relation of the South China Sea precipitation variability between winter and summer. *Climate Dyn.*, **43**, 193–207, doi:10.1007/s00382-013-1820-y.
- Xie, S.-P., K. Hu, J. Hafner, H. Tokinaga, Y. Du, G. Huang, and T. Sampe, 2009: Indian Ocean capacitor effect on Indo–western Pacific climate during the summer following El Niño. *J. Climate*, **22**, 730–747, doi:10.1175/2008JCLI2544.1.
- , Y. Du, G. Huang, X.-T. Zheng, H. Tokinaga, K. Hu, and Q. Liu, 2010: Decadal shift in El Niño influences on Indo–western Pacific and East Asian climate in the 1970s. *J. Climate*, **23**, 3352–3368, doi:10.1175/2010JCLI3429.1.
- , Y. Kosaka, Y. Du, K. Hu, J. S. Chowdary, and G. Huang, 2016: Indo-western Pacific Ocean capacitor and coherent climate anomalies in post-ENSO summer: A review. *Adv. Atmos. Sci.*, **33**, 411–432, doi:10.1007/s00376-015-5192-6.
- Yang, J. L., Q. Y. Liu, S. P. Xie, Z. Y. Liu, and L. X. Wu, 2007: Impact of the Indian Ocean SST basin mode on the Asian summer monsoon. *Geophys. Res. Lett.*, **34**, L02708, doi:10.1029/2006GL028571.
- , —, and Z. Y. Liu, 2010: Linking observations of the Asian monsoon to the Indian Ocean SST: Possible roles of Indian Ocean basin mode and dipole mode. *J. Climate*, **23**, 5889–5902, doi:10.1175/2010JCLI2962.1.
- Zhang, R. H., and R. Huang, 1998: Dynamical effect of zonal wind stresses over the tropical Pacific on the occurring and vanishing of El Niño event: Part I. Diagnostics and theoretical analyses. *Chin. J. Atmos. Sci.*, **22**, 587–599.
- , and A. Sumi, 2002: Moisture circulation over East Asia during El Niño episode in northern winter, spring and autumn. *J. Meteor. Soc. Japan*, **80**, 213–227, doi:10.2151/jmsj.80.213.
- , —, and M. Kimoto, 1999: A diagnostic study of the impact of El Niño on the precipitation in China. *Adv. Atmos. Sci.*, **16**, 229–241, doi:10.1007/BF02973084.
- Zhang, T., and D. Z. Sun, 2014: ENSO asymmetry in CMIP5 models. *J. Climate*, **27**, 4070–4093, doi:10.1175/JCLI-D-13-00454.1.